CENP-E combines a slow, processive motor and a flexible coiled coil to produce an essential motile kinetochore tether

Yumi Kim,[1,2] John E. Heuser,[5] Clare M. Waterman,[6] and Don W. Cleveland[1,3,4]

[1]Ludwig Institute for Cancer Research, [2]Division of Biological Sciences, [3]School of Medicine, and [4]Department of Cellular and Molecular Medicine, University of California, San Diego, La Jolla, CA 92093
[5]Department of Cell Biology, School of Medicine, Washington University, St. Louis, MO 63110
[6]National Heart, Lung, and Blood Institute, National Institutes of Health, Bethesda, MD 20892

The mitotic kinesin centromere protein E (CENP-E) is an essential kinetochore component that directly contributes to the capture and stabilization of spindle microtubules by kinetochores. Although reduction in CENP-E leads to high rates of whole chromosome mis-segregation, neither its properties as a microtubule-dependent motor nor how it contributes to the dynamic linkage between kinetochores and microtubules is known. Using single-molecule assays, we demonstrate that CENP-E is a very slow, highly processive motor that maintains microtubule attachment for long periods. Direct visualization of full-length *Xenopus laevis* CENP-E reveals a highly flexible 230-nm coiled coil separating its kinetochore-binding and motor domains. We also show that full-length CENP-E is a slow plus end–directed motor whose activity is essential for metaphase chromosome alignment. We propose that the highly processive microtubule-dependent motor activity of CENP-E serves to power chromosome congression and provides a flexible, motile tether linking kinetochores to dynamic spindle microtubules.

Introduction

Mitotic chromosome motions are driven by microtubule-based motors positioned at kinetochores as well as by the dynamic properties of spindle microtubules. Centromere protein E (CENP-E) and cytoplasmic dynein are the two microtubule motors in metazoans known to localize at kinetochores (Pfarr et al., 1990; Yen et al., 1992). Each uses chemical energy released from ATP hydrolysis to direct movement toward plus ends or minus ends of microtubules, respectively (Schroer et al., 1989; Wood et al., 1997). Mitotic centromere-associated kinesin, a non-motile kinesin, is also found at the inner centromere, and its microtubule-depolymerizing activity plays a role in error correction so as to generate proper kinetochore microtubule attachment (Desai et al., 1999a; Ohi et al., 2003). Besides the energy-consuming motors, however, energy stored in the microtubule lattice from cleavage of GTP during microtubule assembly can generate sufficient force to power aspects of chromosome movement (Koshland et al., 1988; Coue et al., 1991; Inoue and Salmon, 1995; Grishchuk et al., 2005). By simply maintaining a linkage with spindle microtubules, kinetochores can exploit the energy liberated from the microtubule lattice during disassembly to drive chromosome movement independent of a power stroke generated by motors and additional chemical energy (Howard and Hyman, 2003).

An important unsolved question is how the kinetochore holds onto both growing and shrinking microtubules. Using purified chromosomes attached to dynamic microtubules, either pan kinesin antibodies or those specific for CENP-E were shown to inhibit microtubule depolymerization-dependent motion of chromosomes in vitro (Lombillo et al., 1995a). Moreover, beads coated with kinesin were able to follow the end of disassembling microtubules (Lombillo et al., 1995b), suggesting a role of kinesin family members in coupling kinetochores to dynamic microtubules. Discovery of the ring structure of the yeast Dam1/DASH complex (Miranda et al., 2005; Westermann et al., 2005) has introduced such rings as plausible coupling devices for chromosome attachment and movement. In vitro, the ring complex can move processively on depolymerizing microtubule ends (Westermann et al., 2006), and harness microtubule dynamics to produce force (Asbury et al., 2006). However, the Dam1/DASH complex has not been found outside fungi.

Correspondence to Don W. Cleveland: dcleveland@ucsd.edu

Abbreviations used in this paper: CENP-E, centromere protein E; GMPCPP, guanosine-5′-([a,b]-methyleno) triphosphate; MSD, mean square displacement; TIRF, total internal reflection fluorescence.

The online version of this article contains supplemental material.

The Rockefeller University Press $30.00
J. Cell Biol. Vol. 181 No. 3 411–419
www.jcb.org/cgi/doi/10.1083/jcb.200802189

Conversely, motor enzymes such as dynein, CENP-E, and mitotic centromere-associated kinesin are missing from yeast kinetochores (McIntosh, 2005).

Initially found to be a kinesin family member that localizes to kinetochores (Yen et al., 1992), CENP-E is a mitosis-specific kinesin with a cyclin-like accumulation and degradation, reaching its peak during G2 and early M phase followed by rapid degradation during the completion of mitosis (Brown et al., 1994). As CENP-E is an essential kinetochore component whose loss leads to high rates of whole chromosome missegregation (Weaver et al., 2003), CENP-E is one of the components directly responsible for the stable capture of spindle microtubules by kinetochores (Schaar et al., 1997; Wood et al., 1997; Yao et al., 2000; Putkey et al., 2002). Inhibition or removal of CENP-E not only leads to a failure of metaphase chromosome alignment, resulting in unattached chromosomes that are abnormally close to a spindle pole, but it also reduces the number of microtubules bound by kinetochores even on chromosomes that are bioriented (McEwen et al., 2001; Putkey et al., 2002; Weaver et al., 2003). Most recently, CENP-E has been proposed to facilitate chromosome congression by powering movement of a monooriented chromosome pair toward the spindle equator by attachment to and translocation along the kinetochore fiber of another chromosome pair that had already bioriented (Kapoor et al., 2006). Although simple microtubule gliding assays with the CENP-E motor domain have shown it to be a plus end–directed motor (Wood et al., 1997), the motor properties of CENP-E and the mechanism by which CENP-E contributes to kinetochore attachment to spindle microtubules are not known.

Using purified recombinant CENP-E, we now find that CENP-E is a very slow, highly processive motor that maintains microtubule attachment for long periods with a highly flexible 230-nm-long contour length. These properties combine not only to power chromosome congression but also to provide an essential motile kinetochore tether.

Results and discussion

CENP-E is a slow, processive motor that maintains microtubule attachment for long periods

To characterize the motor properties of CENP-E, we purified the motor plus neck domain of *Xenopus laevis* CENP-E (aa 1–473) with GFP and a hexahistidine tag fused at the C terminus (CE473-GFP hereafter; Fig. 1 A). The presumed dimeric state of this CENP-E fragment was tested by measuring hydrodynamic parameters in solution. A sedimentation coefficient (6 S) and Stokes radius (5.2 nm) were obtained by sucrose gradient sedimentation and gel filtration chromatography, respectively (Fig. S1, A and B; available at http://www.jcb.org/cgi/content/full/jcb.200802189/DC1). This produced a calculated native molecular mass (Siegel and Monty, 1966) for CE473-GFP of ∼130 kD, which is close to the predicted molecular mass of the dimer (160 kD), demonstrating that the preponderance of the CENP-E motor domain exists as a dimer in solution.

We also verified CE473-GFP to be dimeric by using total internal reflection fluorescence (TIRF) microscopy to measure the fluorescence intensity of single molecules immobilized on coverslips. Freshly prepared protein was nonspecifically adhered on a coverslip surface, and the fluorescence intensity of CE473-GFP spots was measured and compared with that of K560-GFP, the well-characterized dimeric motor head of human kinesin-1 (Case et al., 1997). The fluorescence intensity distributions between CE473-GFP (n = 432) and K560-GFP (n = 347) were indistinguishable (Fig. S1 C), confirming that most imaged CENP-E spots were dimers. When the fluorescent CENP-E molecules were followed over time to examine their photobleaching behavior, most CE473-GFP and K560-GFP spots disappeared in either two steps or a single step (Fig. S1 D), as expected if each spot consisted of either two GFPs or a single GFP. Furthermore, the initial fluorescence intensity of moving spots was measured to confirm that the majority of moving CENP-E was indeed dimeric (Fig. S1 E). Therefore, both the hydrodynamic measurements in solution and the fluorescence analysis of single molecules viewed microscopically demonstrate that CE473-GFP is dimeric.

We then tested the processivity of CENP-E in vitro by directly observing single molecules of CE473-GFP moving along microtubules using TIRF microscopy. X-rhodamine–labeled guanosine-5'-([a,b]-methyleno) triphosphate (GMP-CPP) microtubules were immobilized on a coverslip surface using an antitubulin antibody, and, subsequently, a low concentration (0.5–1 nM) of CE473-GFP was introduced into the flow chamber (Fig. 1 B). CENP-E single molecules moved processively and unidirectionally along microtubules (Fig. 1 C and Videos 1 and 2, available at http://www.jcb.org/cgi/content/full/jcb.200802189/DC1) with a median velocity of 8 nm/s (n = 320; four independent preparations; Fig. 1 E). Substantial variation in speed (ranging from 1.7 to 48 nm/s) was observed for CENP-E. However, this was not the result of heterogeneity in motor activity among different protein preparations, as large variation in the velocity was consistently observed in the assays performed on the same day. Furthermore, the velocity of movement often differed by a factor of two even between the molecules running on the same microtubule (Fig. 1 C, compare particle 1 with particle 2).

Processive movement of CENP-E motor single molecules was not smooth, and the CENP-E changed instantaneous velocity with multiple pauses within a single run (Fig. 1 D). Frequent changes in instantaneous velocity with large variations in the speed and even reversals in direction observed when frames were taken more rapidly in our single-molecule assays (Fig. S1, G and H; and Video 3, available at http://www.jcb.org/cgi/content/full/jcb.200802189/DC1) suggested that CENP-E motility has a one-dimensional diffusion component. A mean square displacement (MSD) plot of CENP-E was well fitted with biased Brownian movement (Fig. 1 F). Polynomial regression to MSD (ρ) = $v^2t^2 + 2Dt$ (v, mean drift velocity; D, diffusion coefficient) produced a mean velocity of 9.7 ± 0.6 nm/s (n = 90) and a diffusion coefficient of 690 ± 94 nm^2/s (n = 90), which was larger than expected from the fluctuation of a kinesin with an 8-nm step size and ∼10-nm/s speed (D ≈ 80 nm^2/s; Svoboda et al., 1994).

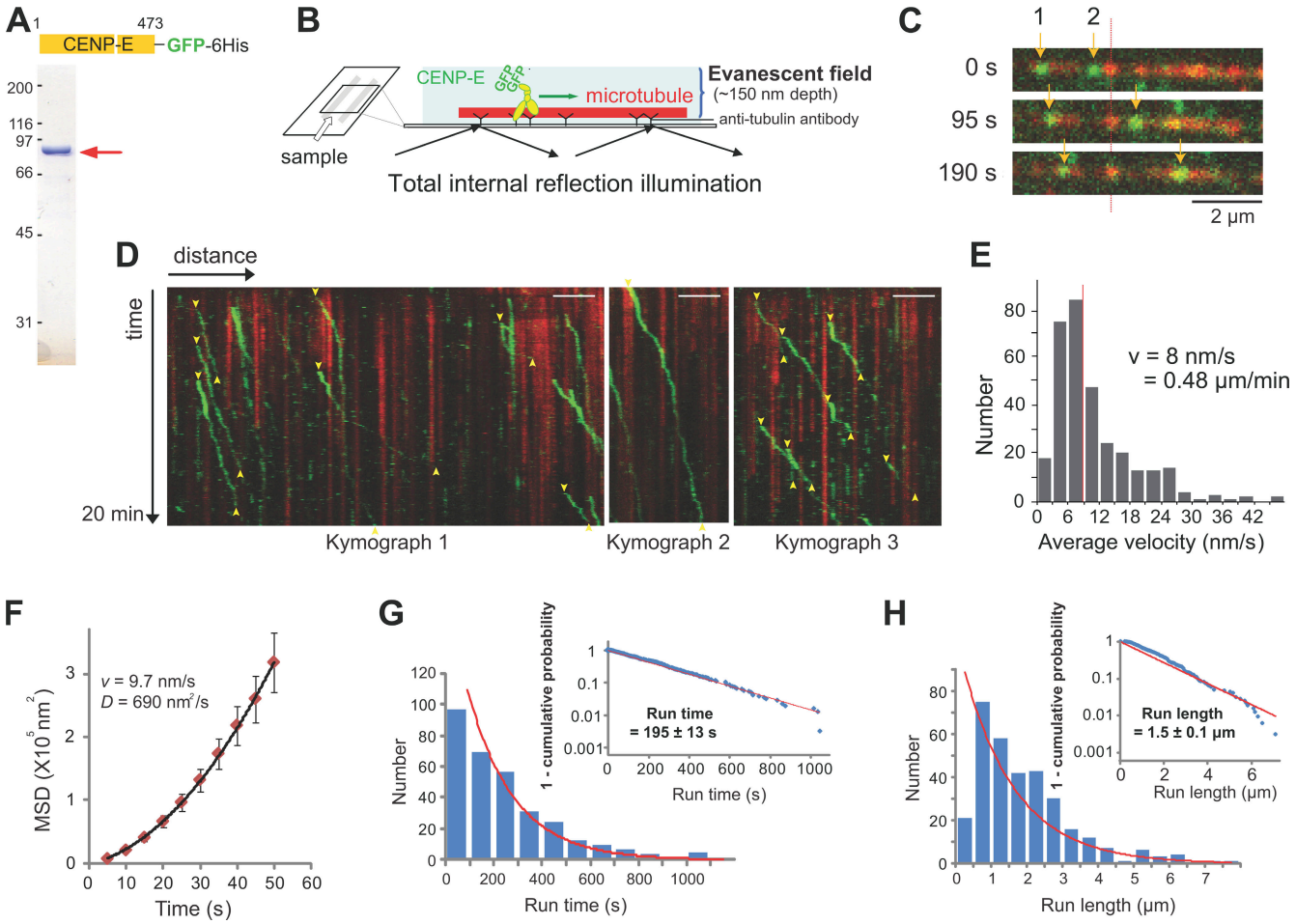

Figure 1. **CENP-E is a slow, processive motor that maintains microtubule attachment for long periods.** (A) Purified CE473-GFP. The arrow points to the purified protein band. (B) Experimental setup for imaging CENP-E single molecules moving along microtubules with TIRF microscopy. X-rhodamine–labeled GMPCPP microtubules were immobilized on a coverslip using antitubulin antibody, and a low concentration of CE473-GFP (0.5–1 nM) was flowed into a flow chamber. (C) Frames from time-lapse imaging of CENP-E motor–GFP moving along microtubules. A fluorescent speckle on the microtubule is indicated with a red line. Two CENP-E molecules moving at different speeds are indicated with arrows. Green, CE473-GFP; red, X-rhodamine–labeled GMPCPP microtubules. (D) Kymographs showing processive movements of the CENP-E motor domain. X-rhodamine speckles on stable microtubules produced vertical red lines. Single molecules of CE473-GFP are shown in green. Yellow arrowheads indicate starts and stops of processive movements. The actual durations of kymographs 1, 2, and 3 were 1,205 s, 1,190 s, and 1,205 s, respectively. (E) Velocity distribution of single CENP-E motor molecules. The median velocity is 8 nm/s (equal to 0.48 μm/min; red line; $n = 320$; four independent preparations). (F) MSD ($\rho(t)$) of CENP-E fitted with $\rho(t) = v^2t^2 + 2Dt$ ($n = 90$). Error bars indicate SEM. (G) The run time of CENP-E motor was distributed exponentially. The mean run time was determined by fitting the data into a cumulative distribution function. The inset shows the one-cumulative probability of CENP-E run time plotted on a log scale. The mean run time is 195 ± 13 s (mean ± SEM; $n = 320$). (H) The run length of CENP-E motor was determined by fitting the data into a cumulative distribution function. The inset shows the one-cumulative probability of CENP-E run length plotted on a log scale. The mean run length is 1.5 ± 0.1 μm (mean ± SEM; $n = 320$). (G and H) Red lines are the exponential fits to the bar graphs. Bars, 2 μm.

Similar mean velocities and diffusion coefficients for CENP-E were found in the experiments performed using more frequent frame rates and quantum dot-labeled CENP-E motor domain (Fig. S1 I).

The presence of a diffusional component in motility has been reported for other microtubule-dependent motors (Vale et al., 1989; Okada and Hirokawa, 1999; Kwok et al., 2006; Helenius et al., 2006; Furuta and Toyoshima, 2008) and suggests that CENP-E contains an additional electrostatic binding mode within the head-neck domain in addition to its force-generating strong microtubule-binding state. This weak binding of CENP-E to a microtubule might prevent the dissociation of CENP-E even when both motors are unbound, thus facilitating efficient reattachment. Consistent with this, CENP-E was able to maintain microtubule attachment for long periods, producing remarkably processive movement despite its slow velocity. The run time, which is defined as the time interval between the start and end of each processive run, was distributed exponentially, and the mean run time was determined by fitting the data into a cumulative distribution function. The mean duration of CENP-E processive runs was 195 ± 13 s (3.3 min; Fig. 1 G), a value 50 times longer than the reported association time of K560-GFP single molecules (Friedman and Vale, 1999). The longest run we observed (Fig. 1 D, kymograph 2) lasted >20 min. The slow velocity and longer association time of the CENP-E motor domain resulted in a mean run length of 1.5 ± 0.1 μm (Fig. 1 H), which is comparable with the processivity of conventional kinesin. Therefore, unlike fast-moving organelle transport kinesins, CENP-E is a slow motor, but its high processivity maintains interaction with a microtubule for long periods.

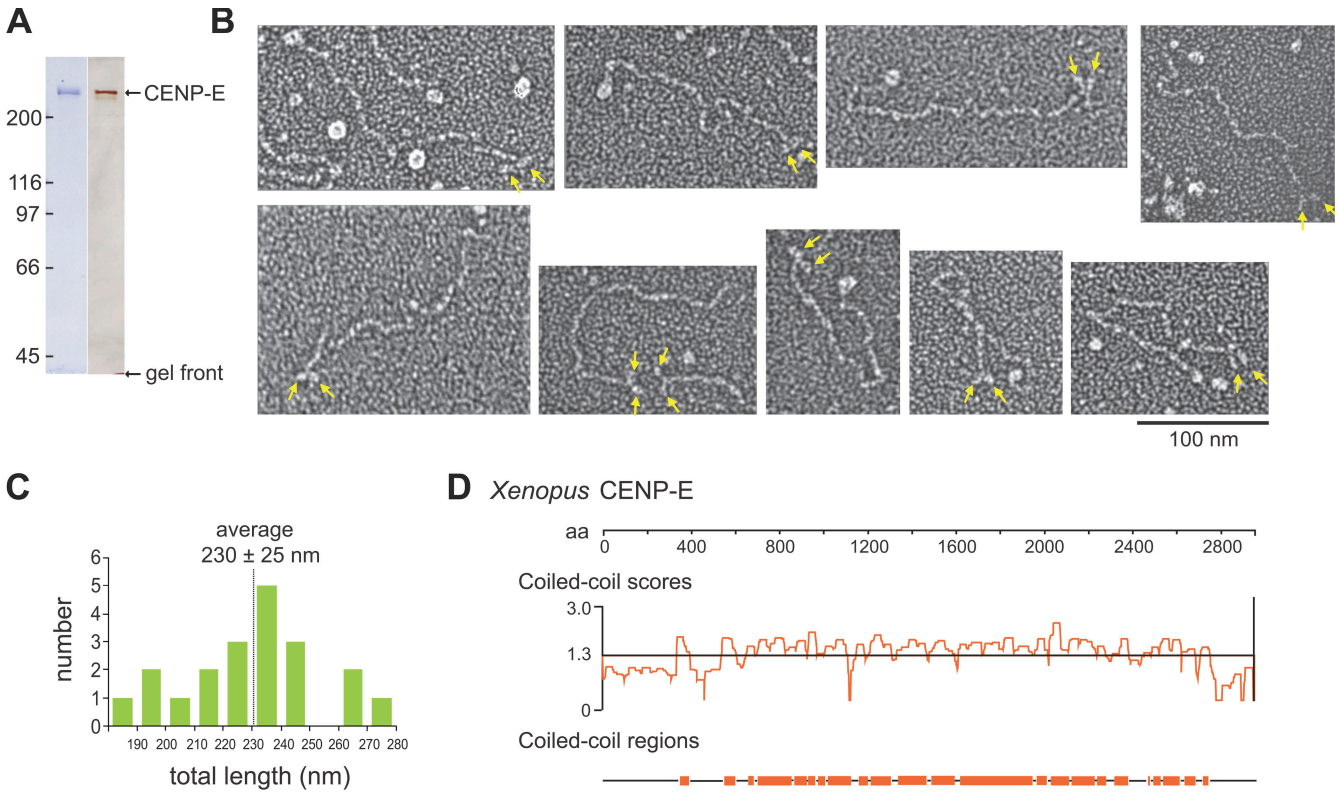

Figure 2. **CENP-E is a highly flexible, dimeric kinesin with a 230-nm discontinuous coiled coil.** (A) Coomassie- and silver-stained *Xenopus* full-length CENP-E (340 kD) purified to near homogeneity from baculovirus-induced insect cells. (B) Electron micrographs of individual CENP-E molecules. Two motor heads are clearly visible, as indicated by yellow arrows. (C) Length distribution of CENP-E. Contour lengths of molecules were measured, and the mean length of CENP-E was 230 ± 25 nm (mean ± SD; $n = 20$). (D) Coiled-coil prediction of *Xenopus* CENP-E. Coiled-coil scores were generated using Protean software (DNAstar) and are graphed below the amino acid scale bar. The number 1.3 is the default value indicating the minimum score for known coiled coils, and resulting predicted coiled-coil domains are shown as solid orange rectangles.

CENP-E is a highly flexible dimeric kinesin with a 230-nm discontinuous coiled coil

To assess the structural features of full-length CENP-E, we purified untagged 340-kD recombinant CENP-E close to homogeneity from insect cells infected with baculovirus-expressing full-length *Xenopus* CENP-E cDNA (Fig. 2 A). Immediately after purification, CENP-E was adsorbed to mica, and individual molecules were visualized by electron microscopy using the quick-freeze deep-etch technique and platinum replication (Heuser, 1989). Consistent with its predicted long α-helical coiled-coil domain, CENP-E was seen to be highly elongated. The two kinesin motor heads, as indicated by arrows, were found separated by a long coiled coil followed by globular tails (Fig. 2 B), directly demonstrating that CENP-E is a homodimer. The mean contour length of CENP-E was measured to be 230 ± 25 nm ($n = 20$; Fig. 2 C), which is almost three times longer than the overall length of conventional kinesin (Hirokawa et al., 1989).

A striking feature of CENP-E was the high flexibility of the α-helical coiled coil, as inferred from the wide variety of configurations that it adopted. Conventional kinesins mainly exist as either extended or folded conformations with a hinge located in the middle of the coiled coil (Hirokawa et al., 1989). In contrast, CENP-E molecules were never uniformly straight but rather displayed a myriad of diverse conformations, none of which could be categorized by frequency as preferred conformations. Throughout the long coiled-coil domain, CENP-E seemed to contain multiple hinges and local distortions that accommodated sharp bends. Analysis of the CENP-E sequence showed that its predicted coiled-coil structure is disrupted >20 times, almost always by segments containing proline or glycine residues (Fig. 2 D). Although it is unknown whether all of the predicted coiled-coil disruptors actually loop out from the coiled-coil axis, the discontinuities in the coiled coil are the mostly likely source of the high flexibility of CENP-E.

Measurement of hydrodynamic properties of full-length CENP-E in solution confirmed a highly elongated, flexible coiled-coil domain. A native molecular mass of 590 kD for recombinant *Xenopus* CENP-E was calculated from the measured values determined by sucrose gradient sedimentation and gel filtration of sedimentation coefficient (8.6 S) and Stokes radius (16 nm), respectively (Fig. S2, A and B; available at http://www.jcb.org/cgi/content/full/jcb.200802189/DC1). This value was close to the predicted molecular mass of a CENP-E homodimer (680 kD), which is consistent with our evidence from electron microscopy that CENP-E is dimeric. Calculating the frictional ratio (f/f_o) using the mass of the dimer (680 kD) and the measured Stokes radius produced a value of 2.8 (Fig. S2 C). If CENP-E were a rigid prolate ellipsoid with an axial ratio of ∼100 (230-nm contour length/2-nm coiled-coil diameter), the f/f_o would be >4. With the f/f_o of 2.8, assuming no hydration and a prolate ellipsoid

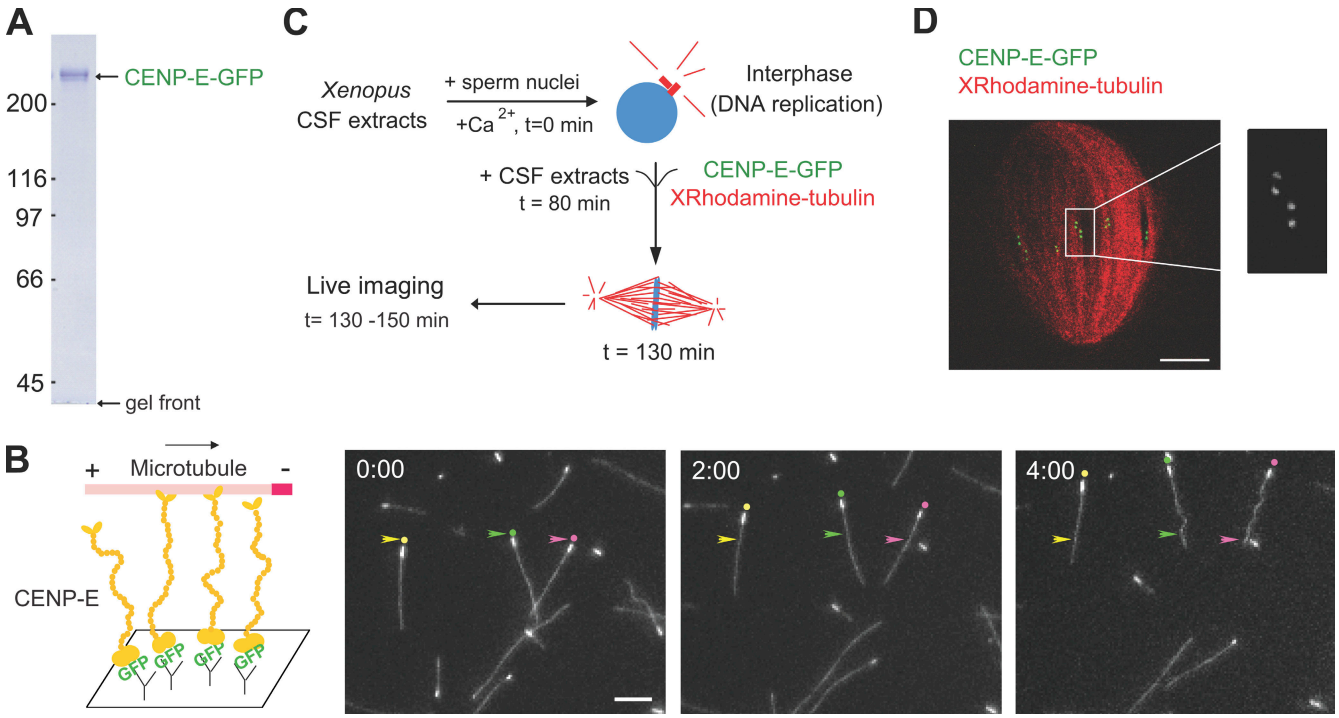

Figure 3. **Full-length CENP-E is a slow plus end–directed kinetochore motor.** (A) Coomassie-stained full-length CENP-E–GFP (366 kD) purified from baculovirus-induced insect cells. (B) Microtubule gliding assay with full-length CENP-E. CENP-E–GFP proteins were tethered to a GFP antibody-coated surface of a flow chamber, and polarity-marked microtubules were subsequently introduced. Minus ends of the microtubules are brightly marked. Colored arrowheads indicate the starting positions of three microtubules, and colored dots indicate the minus ends. The mean gliding velocity was 30 ± 7.6 nm/s (mean ± SD; n = 112). (C) Purified full-length CENP-E–GFP was added into the *Xenopus* extract before spindle assembly. (D) Added CENP-E–GFP was localized to the kinetochore in *Xenopus* extract spindle. A frame from a time-lapse video of a metaphase spindle in the *Xenopus* extracts is shown. Red, X-rhodamine tubulin; green, CENP-E–GFP. Bars: (B) 2 µm; (D) 10 µm.

shape, the maximum possible axial ratio (a/b) of the CENP-E dimer was calculated (Harding and Cölfen, 1995) to be 45 with an estimated length of 148 nm, which is obviously much shorter than CENP-E's actual contour length as determined by electron microscopy. Therefore, CENP-E in solution is substantially elongated on average but is not rigidly extended, which is consistent with the high flexibility observed by electron microscopy.

Full-length CENP-E is a slow plus end–directed kinetochore motor

The characteristics of full-length CENP-E as a motor were determined using polarity-marked fluorescent microtubules and GFP-tagged full-length CENP-E (366 kD) tethered to a coverslip (Fig. 3 A). The directionality of CENP-E has been controversial over the years. Partial purification of native CENP-E was initially reported to contain minus end–directed motility (Thrower et al., 1995), whereas later the recombinant motor domain was shown to be a plus end–directed motor (Wood et al., 1997). It was also reported that native CENP-E purified from mitotic HeLa cells did not support any motility (DeLuca et al., 2001). In this study, we unambiguously show that full-length recombinant CENP-E powered motility toward plus ends of microtubules, with microtubule gliding seen solely with the bright minus end leading. The mean velocity of gliding was 30 ± 7.6 nm/s (n = 112; Fig. 3 B; Video 4, available at http://www.jcb.org/cgi/content/full/jcb.200802189/DC1). Although the speed difference between the motor domain and the full-length CENP-E could reflect autoinhibition of the C-terminal tail binding to the motor domain as recently proposed by Espeut et al. (2008), none of our electron micrographs (Fig. 2 B) offered support for motor binding to the tail of CENP-E.

CENP-E motor activity is essential for metaphase chromosome alignment

It has been well established that CENP-E is essential for stable microtubule capture at the kinetochore and is required for chromosome alignment (Schaar et al., 1997; Wood et al., 1997; Yao et al., 2000; Putkey et al., 2002; Weaver et al., 2003). To test whether it is the motor activity of CENP-E that is essential for chromosome alignment, we used the *Xenopus* egg extract system in which mitotic spindles can be assembled in vitro. When added to *Xenopus* extracts before spindle assembly (Fig. 3 C), CENP-E–GFP localized to kinetochores and remained kinetochore bound throughout metaphase (Fig. 3 D and Video 5, available at http://www.jcb.org/cgi/content/full/jcb.200802189/DC1) and at least until the early stage of anaphase (not depicted).

The contribution of CENP-E motor activity to chromosome alignment and its maintenance was tested by assembling spindles in CENP-E–depleted *Xenopus* extracts that were supplemented with either wild-type CENP-E or motor-dead CENP-E proteins (Fig. 4, A and B). To make a motor-dead CENP-E, we introduced a single point mutation in the ATP-binding P loop (T91N mutation) in the highly conserved kinesin motor domain of CENP-E (Nakata and Hirokawa, 1995).

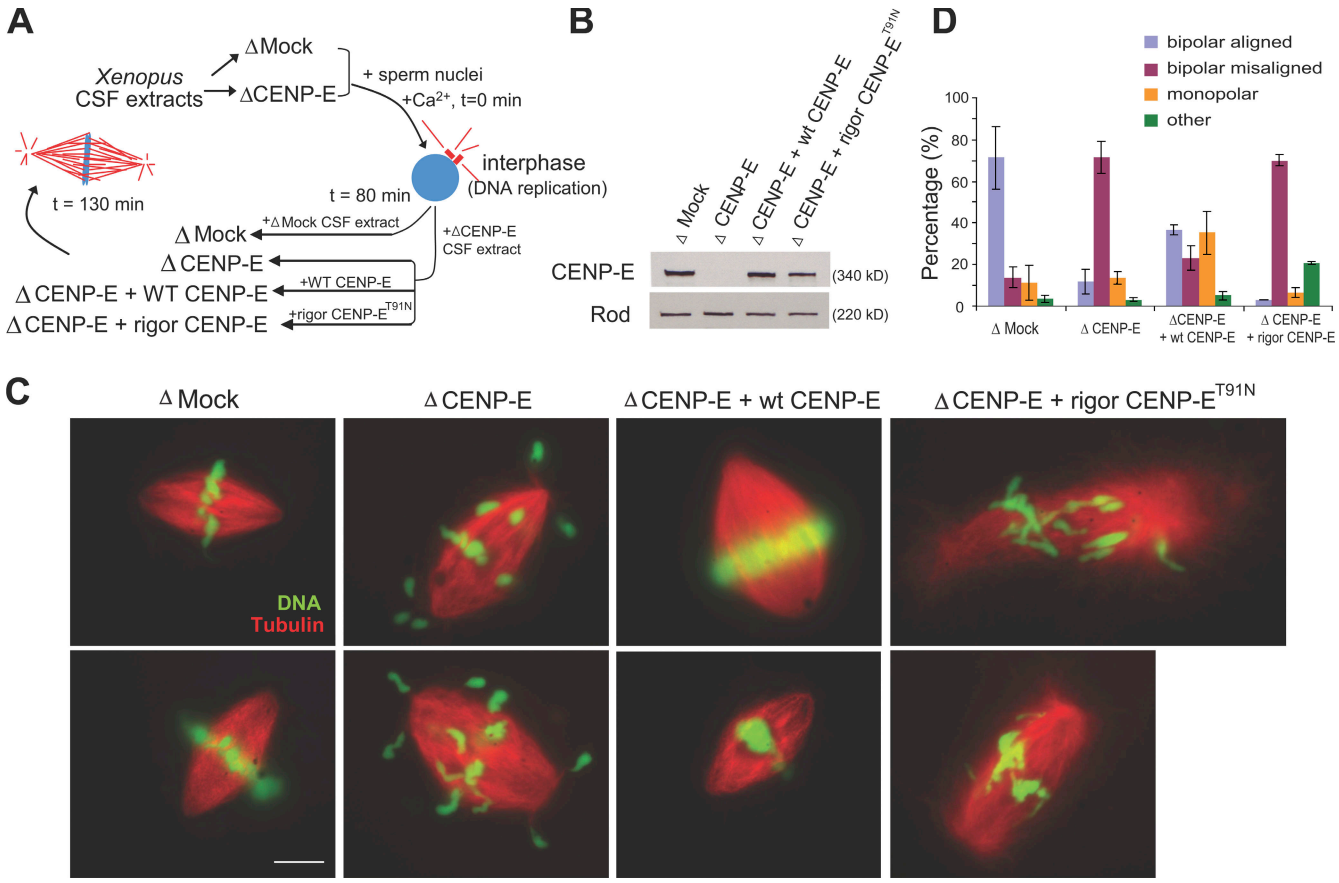

Figure 4. **CENP-E motor activity is essential for metaphase chromosome alignment.** (A) Experimental scheme for *Xenopus* extract manipulation. (B) Immunoblot of CENP-E (340 kD) and Rod (220 kD; a loading control) in mock-depleted, CENP-E–depleted, wild-type CENP-E–supplemented, and rigor CENP-E^{T91N}–supplemented *Xenopus* extracts. (C) Recombinant full-length CENP-E partially rescued chromosome alignment, whereas rigor CENP-E failed at rescue. Red, X-rhodamine tubulin; green, DAPI. (D) Quantification of structures formed in *Xenopus* extracts. More than 200 spindles were scored each in three independent depletion/add-back experiments. Error bars represent SD. Bar, 10 μm.

This mutation provided a rigor binding to microtubules that could not be dissociated even in the presence of ATP, and the motor domain of CENP-E^{T91N} failed to support microtubule gliding even in the presence of saturating ATP concentrations (unpublished data). As reported previously (Wood et al., 1997), chromosomes failed to align properly in the majority of bipolar spindles in CENP-E–depleted extracts (Fig. 4 C). When wild-type CENP-E was added back into CENP-E–depleted extracts before spindle assembly, chromosome alignment defects were rescued in part with the CENP-E localized to kinetochores (Fig. 4, C and D; and Fig. S3, available at http://www.jcb.org/cgi/content/full/jcb.200802189/DC1). Although still bound to kinetochores, rigor CENP-E^{T91N} failed to rescue chromosome alignment, with the chromosomes instead spread along the spindle axis and located close to the spindle poles (Fig. 4, C and D). Accumulation at the broad region of spindle poles in CENP-E^{T91N}–added extracts (Fig. S3) presumably reflected initial rigor binding all along spindle microtubules followed by poleward transport by flux.

Thus, CENP-E motor activity rather than simple microtubule binding is essential for accurate chromosome congression. This conclusion is tempered by the realization that in *Xenopus* extract spindles, chromosomes are prepositioned at the center (precongressed) during spindle assembly, and the process of chromosome alignment may differ from the typical prometaphase congression in somatic cells (Sawin and Mitchison, 1991). Nevertheless, it is clear that the plus end–directed motility of CENP-E, at a minimum, is required for maintenance of chromosome alignment even in a system with fewer required chromosome movements for establishing an initial alignment. We believe that the strong misalignment phenotype from CENP-E depletion in *Xenopus* extracts (Fig. 4), in which fast microtubule poleward flux dominates the forces acting on kinetochores (Maddox et al., 2003a), further supports CENP-E as an essential component for powering plus end–directed chromosome movement to counteract flux.

CENP-E as a motile, flexible kinetochore tether

Use of electron tomography has shown that the vertebrate kinetochore is composed of a fibrous protein network with multiple microtubule interactions (Dong et al., 2007). CENP-E is certainly part of the fibrous network for kinetochore attachment (as demonstrated with immunogold electron microscopy; Cooke et al., 1997; Yao et al., 1997), with its 230-nm length likely to be one of the longest fibers extending out from the kinetochore to capture microtubules. From our evidence, it is now clear that the long coiled coil of CENP-E could work advantageously for the

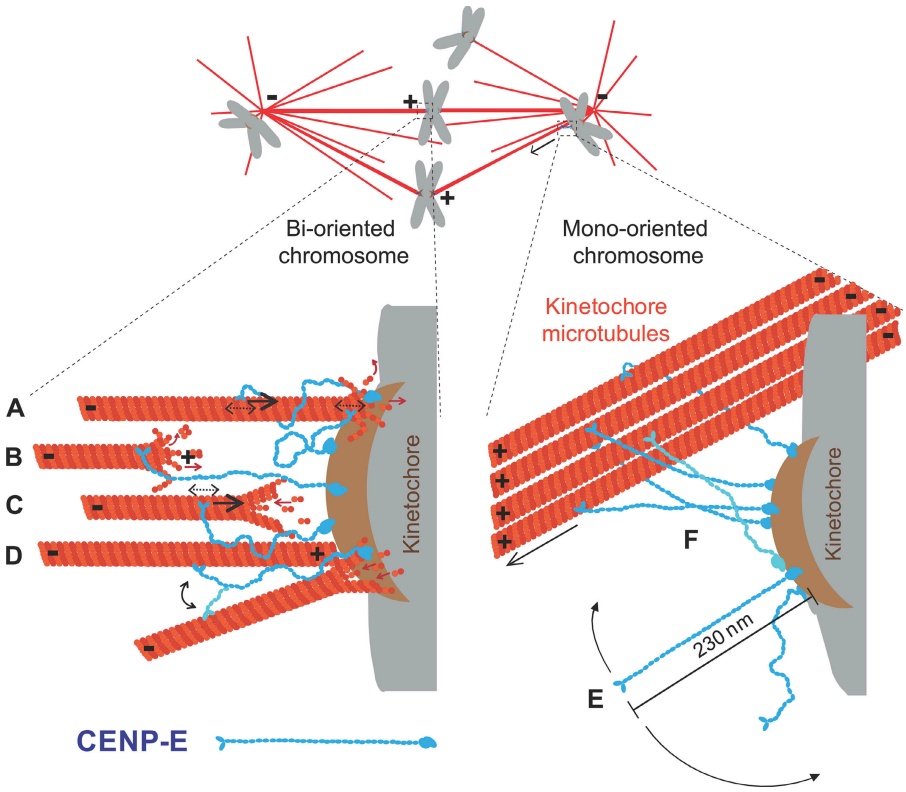

Figure 5. **A model for CENP-E as a motile, flexible tether for kinetochore microtubule capture and maintenance of linkage to dynamic spindle microtubules.** (A) Using its slow processive motor activity and a weak diffusive binding mode to microtubules, CENP-E walks toward the plus ends of kinetochore microtubules or diffuses along the lattice without dissociating for extended periods. (B) The 230-nm-long coiled coil of CENP-E functions as a safety catch for disassembling microtubules detached from the core kinetochore attachment components, thereby stabilizing the microtubule and enabling rescue. (C) CENP-E is likely to be a part of the kinetochore slip clutch that is engaged on fluxing kinetochore microtubules with its slow plus end–directed motility (Maddox et al., 2003a). CENP-E bound to the microtubule surface may affect kinetochore microtubule plus ends, thereby promoting growth and allowing recapture. (D) Unlike other shorter and more rigidly structured kinetochore capture components, multiple CENP-E molecules are likely to work together by allowing the simultaneous attachment at many different microtubule orientations relative to the kinetochore axis without forcing each other into unproductive conformations. (E) The highly flexible extended coiled coil of CENP-E mediates the initial capture of microtubules by searching a large volume in cells. (F) Its slow, processive motility powers monooriented chromosomes to congress using an adjacent kinetochore fiber (Kapoor et al., 2006).

initial capture of kinetochores to spindle microtubules by searching a large radial volume in cells (Fig. 5 E). After initial capture, the combination of slow processive movement along with one-dimensional diffusion would yield the translocation of CENP-E to the plus ends of microtubules, potentially damping dynamics there (Fig. 5 A). An important novel aspect is that the high flexibility would allow versatile configurations of CENP-E binding to microtubules, permitting kinetochore attachment to microtubules approaching from a wide range of angles (Fig. 5, D and F). This would be in contrast to the highly conserved Ndc80 complex, which has been implicated as a key nonmotor microtubule-binding component of kinetochores (Ciferri et al., 2007) and whose ~55-nm stiff rod (Wei et al., 2005) apparently binds with a consistent polarity at a fixed angle relative to the microtubule lattice (Cheeseman et al., 2006).

Finally, the 230-nm-long coiled coil of CENP-E is long enough to cover the entire kinetochore region and could even reach over to kinetochore fibers of other chromosomes passing close by (Fig. 5 F). Our evidence supports that CENP-E, as a highly processive kinesin, is capable of driving the congression of a monooriented chromosome to the center along the neighboring kinetochore fibers (Kapoor et al., 2006). Indeed, the speed of microtubule gliding driven by multiple CENP-E molecules immobilized on a coverslip is similar to what has been observed for the velocities of kinetochore motility during chromosome congression in cells (Fig. 3 D; Skibbens et al., 1993). Furthermore, the high flexibility of CENP-E would allow multiple molecules to work together along the kinetochore fibers without forcing each other into unproductive conformations.

The CENP-E family kinesin (kinesin-7) has a longer family-specific neck domain than conventional kinesins (Endow, 1999). We hypothesize that the longer neck and highly flexible, discontinuous coiled-coil domain of CENP-E are specialized for three roles during mitosis: efficient microtubule capture by kinetochores, towing monooriented chromosomes through viscous cytoplasm (especially those initially far from the spindle equator), and, perhaps most importantly, as a motile kinetochore tether maintaining linkage to dynamic kinetochore microtubule plus ends. The last of these properties couples the slow, processive motility with one-dimensional diffusion that together offer a molecular explanation for how relatively few CENP-E molecules (~50 dimers per human kinetochore; Brown et al., 1994) can sustain kinetochore attachment to individual dynamic (growing and shrinking) microtubules without losing connection. Combined with the highly flexible 230-nm-long coiled coil, slow plus end–directed motility, and ability of single molecules to remain microtubule bound for minutes, we propose that CENP-E is a part of the kinetochore slip clutch that is engaged on fluxing kinetochore microtubules (Maddox et al., 2003a). In effect, CENP-E combines a slow but processive motor, flexibility, reach, and stable microtubule binding to produce a motile molecular Velcro at kinetochores (Fig. 5).

Materials and methods

Cloning, expression, and purification of CENP-E

cDNA encoding *Xenopus* CENP-E residues 1–473 fused at the C terminus to a GFP-6His tag was cloned into pET23d (Novagen), and protein expression was induced at 13°C for ~12 h with 10 nM IPTG in Rosetta (DE3). Bacterial pellets were suspended in lysis buffer (25 mM K-Pipes, pH 6.8, 300 mM KCl, 40 mM imidazole, 2 mM $MgCl_2$, 0.5 mM EGTA, 10 mM β-mercaptoethanol, 0.1 mM ATP, 1 mM PMSF, and protease inhibitors [from cocktail tablet; Roche]) and lysed by sonication after lysozyme treatment (1 mg/ml) on ice for 30 min. After centrifugation at 15,000 rpm (SA-600; Sorvall) for 30 min, the supernatant was incubated with Ni–nitrilotriacetic acid

(QIAGEN) for 1 h at 4°C. The protein was further purified by HiTrap SP HP (GE Healthcare) using 100 mM–1 M KCl gradient elution in 25 mM Pipes, pH 6.8, 2 mM $MgCl_2$, 1 mM DTT, and 0.1 mM ATP. The peak fraction from the sulphopropyl column was then loaded onto Superose 6 10/300 (GE Healthcare) preequilibrated with the same buffer containing 100 mM KCl, and the peak fraction was used in the assay.

Full-length *Xenopus* CENP-E (340 kD) and CENP-E–GFP (366 kD) were expressed and purified from High Five cells (Invitrogen) as previously described (Abrieu et al., 2000) followed by a final purification with a Superose 6 column. To make rigor CENP-E, the Thr at residue 91 was mutated to Asn (ACG → AAC) using site-directed mutagenesis. Fresh proteins were used in all experiments with the exception of the *Xenopus* extracts experiment.

Sucrose gradient sedimentation and gel filtration chromatography

To measure the S value of CENP-E, 100 µl of protein was centrifuged through 2 ml of 5–40% sucrose gradients at 50,000 rpm for 6 h at 4°C (TLS 55 rotor; Beckman Coulter). The sedimentation coefficient of CENP-E was determined by linear interpolation of a standard curve (R^2 = 0.96) using proteins of known S values (BSA, 4.6 S; aldolase, 7.3 S; catalase, 11.3 S; thyroglobulin, 19 S). To measure the Stokes radius of full-length CENP-E, Sephacryl S-500 HR (GE Healthcare) was packed into a column (XK 26/70; GE Healthcare) calibrated with protein standards (20 nm myosin II, 12.5 nm IgM, 8.5 nm thyroglobulin, 5.2 nm catalase, and 4.8 nm aldolase; R^2 = 0.99). 500 µl of partially purified protein was loaded, and CENP-E was detected by immunoblotting. The partial specific volume (υ) of CENP-E was calculated to be 0.735 cm^3/g from the mean partial specific volumes of the individual amino acids as described by Perkins (1986). Native molecular weight and frictional ratio (f/f_o) were calculated as described previously (Siegel and Monty, 1966). The maximum possible axial ratio was calculated as described in Harding and Cölfen (1995) assuming no hydration and a prolate ellipsoid. The dimensions for CENP-E were calculated from the volume of a spherical mass of 680 kD and the partial specific volume, with $V = \upsilon \times M/A = (4/3)\ \pi\ ab^2$, where M represents molecular weight, A represents Avogadro's number (6.02×10^{23}), and a = 45b.

Single-molecule assays

CENP-E single-molecule assays were performed at room temperature using a digital TIRF imaging system described in detail in Adams et al. (2004). In brief, this consisted of a microscope (TE2000-U; Nikon) equipped with a custom-modified TIRF epiilluminator and a 100× NA 1.45A TIRF objective (Nikon). Illumination for TIRF imaging of GFP and X-rhodamine was provided by the 488- and 568-nm lines of a 50-mW KrAr laser, with individual lines selected by a polychromatic acousto-optic modulator (Neos Technologies). TIRF images using an evanescent field illumination depth of 150 nm were captured using an electron-multiplying CCD camera (Cascade II; Photometrics). Microscope automation, image acquisition, and processing were performed using MetaMorph software (MDS Analytical Technologies). Flow cells were constructed with a slide and 22 × 22-mm square coverslip separated by two strips of double-stick tape. For measuring fluorescence intensity and photobleaching, ∼0.5 nM of motors was incubated for 10 min. Fluorescence intensity was measured by integrating the signal of a fluorescent spot per frame and subtracting the background (integrated area = 49 $pixel^2$). For motility assays, 50 µg/ml of a rat monoclonal tubulin antibody (Serotec) was incubated for 5 min followed by BRB80 (80 mM K-Pipes, pH 6.8, 1 mM $MgCl_2$, and 1 mM EGTA) wash, X-rhodamine–labeled GMPCPP microtubules for 10 min, and 0.5 mg/ml casein-blocking solution for 10 min. Then, ∼0.5–1 nM CENP-E motor in motility buffer with an oxygen scavenging system (BRB80, 1 mM DTT, 3 mM ATP, 4.5 mg/ml glucose, 0.2 mg/ml glucose oxidase, and 35 ug/ml catalase) was flowed into the chamber. Frames were captured every 5 s with 120-ms exposure (three frames with 40-ms exposure were averaged to increase the signal to noise ratio), and the duration of imaging was ∼5–20 min, which results in a total exposure of ∼7.2–28.8 s. Events that lasted more than two frames (>10 s) were tracked, and nonmoving molecules were excluded from our analysis. CENP-E processive runs were analyzed by drawing kymographs with MetaMorph (MDS Analytical Technologies), and for MSD analyses, the intensity centroid of moving CENP-E spots was tracked using the MetaMorph Track Object tool. Particle coordinates ($x_n = x(n\Delta T)$ and $y_n = y(n\Delta T)$) were used to calculate MSD: $(\rho_n) = \rho(n\Delta T) =$

$$\sum_{i=0}^{N} (x_{i+n} - x_i)^2 / (N+1) + \sum_{i=0}^{N} (y_{i+n} - y_i)^2 / (N+1),$$

where ΔT is the data acquisition time interval (Qian et al., 1991). MSD was fitted with the equation for biased Brownian movement: MSD (ρ) = $\upsilon^2 t^2 + 2Dt$ (D, diffusion coefficient; υ, mean velocity).

Microtubule gliding assay

Microtubule gliding assays were performed as described previously (Wood et al., 1997) with use of GFP antibody to coat CENP-E–GFP onto a coverslip. Time-lapse image acquisition was performed at room temperature using an inverted microscope (Eclipse TE 300; Nikon) with a 60× NA 1.4A objective, and the images were captured with a camera (CoolSNAP HQ; Photometrics) controlled by MetaMorph.

Electron microscopy

Freshly prepared CENP-E was maintained on ice overnight and processed for freeze drying the following morning. CENP-E proteins were adsorbed to a suspension of mica flakes followed by freeze drying and platinum replication (Heuser, 1989).

Spindle assembly, live imaging, and immunofluorescence in *Xenopus* extract

The preparation of *Xenopus* cytostatic factor–arrested egg extracts and the cycled spindle assembly in vitro were performed as described previously (Desai et al., 1999b). For live imaging, ∼5 ug/ml X-rhodamine tubulin and 25 nM of recombinant CENP-E–GFP were added in the *Xenopus* extracts before spindle assembly, and squashed extract was imaged using a spinning disk confocal mounted on a microscope (TE2000e; Nikon) with a 100× NA 1.4A objective (Nikon) and 2 × 2 binning as described in Maddox et al. (2003b). CENP-E immunodepletion and immunofluorescence were performed as described previously (Abrieu et al., 2000). More than 95% of CENP-E was consistently depleted using this method. For rescue experiments, either wild-type or rigor $CENP\text{-}E^{T91N}$ protein was added to CENP-E–depleted extract at endogenous level (∼25 nM) after completion of DNA replication.

Online supplemental material

Fig. S1 shows that CE473-GFP forms a dimer. Fig. S2 shows hydrodynamic measurements demonstrating that purified full-length CENP-E in solution is dimeric with high flexibility. Fig. S3 shows CENP-E localization in the *Xenopus* extract spindles in Fig. 4. Video 1 shows processive movements of CE473-GFP, and Video 2 shows processive movements of Qdot525-labeled CENP-E (aa 1–473). Video 3 shows backward movement of Qdot525-labeled CENP-E (aa 1–473). Video 4 shows a microtubule gliding assay with CENP-E–GFP (366 kD) and polarity-marked microtubules. Video 5 shows that recombinant CENP-E–GFP is localized to kinetochores in *Xenopus* extract spindles. Online supplemental material is available at http://www.jcb.org/cgi/content/full/jcb.200802189/DC1.

We are grateful to Arshad Desai (University of California, San Diego, La Jolla, CA) for advice and reagents for assembling microtubules, Paul Maddox for encouragement, Ian Schneider for help with TIRF imaging, Robyn Roth for help with EM, Ron Vale (University of California, San Francisco, San Francisco, CA) for providing K560-GFP construct, and members of the Cleveland laboratory for stimulating discussions.

This work was supported by a National Institutes of Health grant (GM29513) to D.W. Cleveland. Salary support for D.W. Cleveland is provided by the Ludwig Institute for Cancer Research.

Submitted: 28 February 2008
Accepted: 1 April 2008

References

Abrieu, A., J.A. Kahana, K.W. Wood, and D.W. Cleveland. 2000. CENP-E as an essential component of mitotic checkpoint in vitro. *Cell.* 102:817–826.

Adams, M.C., A. Matov, D. Yarar, S.L. Gupton, G. Danuser, and C.M. Waterman-Storer. 2004. Signal analysis of total internal reflection fluorescent speckle microscopy (TIR-FSM) and widefield epi-fluorescence FSM of the actin cytoskeleton and focal adhesions in living cells. *J. Microsc.* 216:138–152.

Asbury, C.L., D.R. Gestaut, A.F. Powers, A.D. Franck, and T.N. Davis. 2006. The Dam1 kinetochore complex harness microtubule dynamics to produce force and movement. *Proc. Natl. Acad. Sci. USA.* 103:9873–9878.

Brown, K.D., R.M.R. Coulson, T.J. Yen, and D.W. Cleveland. 1994. Cyclin-like accumulation and loss of the putative kinetochore motor CENP-E results from coupling continuous synthesis with specific degradation at the end of mitosis. *J. Cell Biol.* 125:1303–1312.

Case, R.B., D.W. Pierce, N. Hom-Booher, C.L. Hart, and R.D. Vale. 1997. The directional preference of kinesin motors is specified by an element outside of the motor catalytic domain. *Cell.* 90:959–966.

Cheeseman, I.M., J.S. Chappie, E.M. Wilson-Kubalek, and A. Desai. 2006. The conserved KMN network constitutes the core microtubule-binding site of the kinetochore. *Cell.* 127:983–997.

Ciferri, C., A. Musacchio, and A. Petrovic. 2007. The Ndc80 complex: Hub of kinetochore activity. *FEBS Lett.* 581:2862–2869.

Cooke, C.A., B. Schaar, T.J. Yen, and W.C. Earnshaw. 1997. Localization of CENP-E in the fibrous corona and outer plate of mammalian kinetochores from prometaphase through anaphase. *Chromosoma.* 106:446–455.

Coue, M., V.A. Lombillo, and J.R. McIntosh. 1991. Microtubule depolymerization promotes particle and chromosome movement in vitro. *J. Cell Biol.* 112:1165–1175.

DeLuca, J.G., C.N. Newton, R.H. Himes, M.A. Jordan, and L. Wilson. 2001. Purification and characterization of native conventional kinesin, HSET, and CENP-E from mitotic hela cells. *J. Biol. Chem.* 276:28014–28021.

Desai, A., S. Verma, T.J. Mitchison, and C.E. Walczak. 1999a. Kin I kinesins are microtubule-destabilizing enzymes. *Cell.* 96:69–78.

Desai, A., A. Murray, T.J. Mitchison, and C.E. Walczak. 1999b. The use of *Xenopus* egg extracts to study mitotic spindle assembly and function in vitro. *Methods Cell Biol.* 61:385–412.

Dong, Y., K.J. VandenBeldt, X. Meng, A. Khodjakov, and B.F. McEwen. 2007. The outer plate in vertebrate kinetochores is a flexible network with multiple microtubule interactions. *Nat. Cell Biol.* 9:516–522.

Endow, S.A. 1999. Determinants of molecular motor directionality. *Nat. Cell Biol.* 1:E163–E167.

Espeut, J., A. Gaussen, P. Bieling, V. Morin, S. Prieto, D. Fesquet, T. Surrey, and A. Abrieu. 2008. Phosphorylation relieves autoinhibition of the kinetochore motor CENP-E. *Mol. Cell.* 29:637–643.

Friedman, D.S., and R.D. Vale. 1999. Single-molecule analysis of kinesin motility reveals regulation by the cargo-binding tail domain. *Nat. Cell Biol.* 1:293–297.

Furuta, K., and Y.Y. Toyoshima. 2008. Minus-end-directed motor Ncd exhibits processive movement that is enhanced by microtubule bundling in vitro. *Curr. Biol.* 18:152–157.

Grishchuk, E.L., M.I. Molodtsov, F.I. Ataullakhanov, and J.R. McIntosh. 2005. Force production by disassembling microtubules. *Nature.* 438:384–388.

Harding, S.E., and H. Cölfen. 1995. Inversion formulae for ellipsoid of revolution macromolecular shape functions. *Anal. Biochem.* 228:131–142.

Helenius, J., G. Brouhard, Y. Kalaidzidis, S. Diez, and J. Howard. 2006. The depolymerizing kinesin MCAK uses lattice diffusion to rapidly target microtubule ends. *Nature.* 441:115–119.

Heuser, J. 1989. Protocol for 3-D visualization of molecules on mica via the quick-freeze, deep-etch technique. *J. Electron Microsc. Tech.* 13:244–263.

Hirokawa, N., H. Yorifuji, M.C. Wagner, S.T. Brady, and G.S. Bloom. 1989. Submolecular domains of bovine brain kinesin identified by electron microscopy and monoclonal antibody decoration. *Cell.* 56:867–878.

Howard, J., and A.A. Hyman. 2003. Dynamics and mechanics of the microtubule plus ends. *Nature.* 422:753–758.

Inoue, S., and E.D. Salmon. 1995. Force generation by microtubule assembly/disassembly in mitosis and related movement. *Mol. Biol. Cell.* 6:1619–1640.

Kapoor, T.M., M.A. Lampson, P. Hergert, L. Cameron, D. Cimini, E.D. Salmon, B.F. McEwen, and A. Khodjakov. 2006. Chromosomes can congress to the metaphase plate before biorientation. *Science.* 311:388–391.

Koshland, D.E., T.J. Mitchison, and M.W. Kirschner. 1988. Polewards chromosome movement driven by microtubule depolymerization in vitro. *Nature.* 331:499–504.

Kwok, B.H., L.C. Kapitein, J.H. Kim, E.J.G. Peterman, C.F. Schimidt, and T.M. Kapoor. 2006. Allosteric inhibition of kinesin-5 modulates its processive directional motility. *Nat. Chem. Biol.* 2:480–485.

Lombillo, V.A., C. Nislow, T.J. Yen, V.I. Gelfand, and J.R. McIntosh. 1995a. Antibodies to the kinesin motor domain and CENP-E inhibit microtubule depolymerization-dependent motion of chromosomes in vitro. *J. Cell Biol.* 128:107–115.

Lombillo, V.A., R.J. Stewart, and J.R. McIntosh. 1995b. Minus-end-directed motion of kinesin-coated microspheres driven by microtubule depolymerization. *Nature.* 373:161–164.

Maddox, P., A. Straight, P. Coughlin, T.J. Mitchison, and E.D. Salmon. 2003a. Direct observation of microtubule dynamics at kinetochores in *Xenopus* extract spindles: implications for spindle mechanics. *J. Cell Biol.* 162:377–382.

Maddox, P.S., B. Moree, J.C. Canman, and E.D. Salmon. 2003b. Spinning disk confocal microscope system for rapid high-resolution, multimode, fluorescence speckle microscopy and green fluorescent protein imaging in living cells. *Methods Enzymol.* 360:597–617.

McEwen, B.F., G.K.T. Chan, B. Zubrowski, M.S. Savoian, M.T. Sauer, and T.J. Yen. 2001. CENP-E is essential for reliable bioriented spindle attachment, but chromosome alignment can be achieved via redundant mechanisms in mammalian cells. *Mol. Biol. Cell.* 12:2776–2789.

McIntosh, J.R. 2005. Rings around kinetochore microtubules in yeast. *Nat. Struct. Mol. Biol.* 12:210–212.

Miranda, J.J.L., P.D. Wulf, P.K. Sorger, and S.C. Harrison. 2005. The yeast DASH complex forms closed rings on microtubules. *Nat. Struct. Mol. Biol.* 12:138–143.

Nakata, T., and N. Hirokawa. 1995. Point mutation of adenosine triphosphate-binding motif generated rigor kinesin that selectively blocks anterograde lysosome membrane transport. *J. Cell Biol.* 131:1039–1053.

Ohi, R., M.L. Coughlin, W.S. Lane, and T.J. Mitchison. 2003. An inner centromere protein that stimulates the microtubule depolymerizing activity of a KinI kinesin. *Dev. Cell.* 5:309–321.

Okada, Y., and N. Hirokawa. 1999. A processive single-headed motor: kinesin superfamily protein Kif1a. *Science.* 283:1152–1157.

Perkins, S.J. 1986. Protein volumes and hydration effects. The calculations of partial specific volumes, neutron scattering matchpoints and 280-nm absorption coefficients for proteins and glycoproteins from amino acid sequences. *Eur. J. Biochem.* 157:169–180.

Pfarr, C.M., M. Coue, P.M. Grissom, T.S. Hays, M.E. Porter, and J.R. McIntosh. 1990. Cytoplasmic dynein is localized to kinetochores during mitosis. *Nature.* 345:263–265.

Putkey, F.R., T. Cramer, M.K. Morphew, A.D. Silk, R.S. Johnson, J.R. McIntosh, and D.W. Cleveland. 2002. Unstable kinetochore-microtubule capture and chromosomal instability following deletion of CENP-E. *Dev. Cell.* 3:351–365.

Qian, H., M.P. Sheetz, and E.L. Elson. 1991. Single particle tracking, Analysis of diffusion and flow in two-dimensional systems. *Biophys. J.* 60:910–921.

Sawin, K.E., and T.J. Mitchison. 1991. Mitotic spindle assembly by two different pathways in vitro. *J. Cell Biol.* 112:925–940.

Schaar, B.T., G.K.T. Chan, P. Maddox, E.D. Salmon, and T.J. Yen. 1997. CENP-E function at kinetochores is essential for chromosome alignment. *J. Cell Biol.* 139:1373–1382.

Schroer, T.A., E.R. Steuer, and M.P. Sheetz. 1989. Cytoplasmic dynein is a minus end-directed motor for membranous organelles. *Cell.* 56:937–946.

Siegel, L.M., and K.J. Monty. 1966. Determination of molecular weights and frictional ratios of proteins in impure systems by use of gel filtration and density gradient centrifugation. Application to crude preparations of sulfate and hydroxylamine reductases. *Biochim. Biophys. Acta.* 112:346–362.

Skibbens, R.V., V.P. Skeen, and E.D. Salmon. 1993. Directional instability of kinetochore motility during chromosome congression and segregation in mitotic newt lung cells: a push-pull mechanism. *J. Cell Biol.* 122:859–875.

Svoboda, K., P.P. Mitra, and S.M. Block. 1994. Fluctuation analysis of motor protein movement and single enzyme kinetics. *Proc. Natl. Acad. Sci. USA.* 91:11782–11786.

Thrower, D.A., M.A. Jordan, B.T. Schaar, T.J. Yen, and L. Wilson. 1995. Mitotic HeLa cells contain a CENP-E-associated minus end-directed microtubule motor. *EMBO J.* 14:918–926.

Vale, R.D., D.R. Soll, and I.R. Gibbons. 1989. One-dimensional diffusion of microtubules bound to flagella dynein. *Cell.* 59:915–925.

Weaver, B.A., Z.Q. Bonday, F.R. Putkey, G.J.P.L. Kops, A.D. Silk, and D.W. Cleveland. 2003. Centromere-associated protein-E is essential for the mammalian mitotic checkpoint to prevent aneuploidy due to single chromosome loss. *J. Cell Biol.* 162:551–563.

Wei, R.R., P.K. Sorger, and S.C. Harrison. 2005. Molecular organization of the Ndc80 complex, an essential kinetochore component. *Proc. Natl. Acad. Sci. USA.* 102:5363–5367.

Westermann, S., A. Avila-Saker, H. Wang, H. Niederstrasser, J. Wong, D.G. Drubin, E. Nogales, and G. Barnes. 2005. Formation of a dynamic kinetochore-microtubule interface through assembly of the Dam1 ring complex. *Mol. Cell.* 17:277–290.

Westermann, S., H.-W. Wang, A. Avila-Sakar, D. Drubin, E. Nogales, and G. Barnes. 2006. The Dam1 kinetochore ring complex moves processively on depolymerizing microtubule ends. *Nature.* 440:565–569.

Wood, K.W., R. Sakowicz, L.S. Goldstein, and D.W. Cleveland. 1997. CENP-E is a plus end-directed kinetochore motor required for metaphase chromosome alignment. *Cell.* 91:357–366.

Yao, X., K.L. Anderson, and D.W. Cleveland. 1997. The microtubule-dependent motor centromere-associated protein E (CENP-E) is an integral component of kinetochore corona fibers that link centromeres to spindle microtubules. *J. Cell Biol.* 139:435–447.

Yao, X., A. Abrieu, Y. Zheng, K.F. Sullivan, and D.W. Cleveland. 2000. CENP-E forms a link between attachment of spindle microtubules to kinetochores and the mitotic checkpoint. *Nat. Cell Biol.* 2:484–491.

Yen, T.J., G. Li, B.T. Scharr, I. Szilak, and D.W. Cleveland. 1992. CENP-E is a putative kinetochore motor that accumulates just before mitosis. *Nature.* 359:536–539.